molecular pharmaceutics

Article

Cite This: Mol. Pharmaceutics 2018, 15, 3871−3880

pubs.acs.org/molecularpharmaceutics

Catalytic Reaction Mechanism for Drug Metabolism in Human Carboxylesterase-1: Cocaine Hydrolysis Pathway

Jianzhuang Yao,[†,§,⊥] Xiabin Chen,[‡,∥,⊥] Fang Zheng,[*,§,∥] and Chang-Guo Zhan[*,§,∥]

[†]School of Biological Science and Techonology, University of Jinan, Jinan 250022, China

[‡]School of Medicine, Hangzhou Normal University, Hangzhou 311121, China

[§]Molecular Modeling and Biopharmaceutical Center and [∥]Department of Pharmaceutical Sciences, College of Pharmacy, University of Kentucky, 789 South Limestone Street, Lexington, Kentucky 40536, United States

Supporting Information

ABSTRACT: Carboxylesterase-1 (CE-1) is a crucial enzyme responsible for metabolism/activation/inactivation of xenobiotics (therapeutic agents, prodrugs, abused drugs, and organophosphorus nerve agents *etc.*) and also involved in many other biological processes. In this study, we performed extensive computational modeling and simulations to understand the fundamental reaction mechanism of cocaine hydrolysis catalyzed by CE-1, revealing that CE-1-catalyzed cocaine hydrolysis follows a novel reaction pathway with only two reaction steps: a single-step acylation process and a single-step deacylation process. In the transition states of both single-step processes, the cocaine NH group joins the oxyanion hole to form an additional hydrogen bond with the negatively charged carbonyl oxygen atom of the cocaine. Thus, the transition states are stabilized by both intermolecular and intramolecular hydrogen bonds with the methyl ester of cocaine, specifically the carbonyl oxygen atom. The rate-limiting transition state is associated with the acylation process, and the activation free energy barrier was predicted to be 20.1 kcal/mol. Further, *in vitro* experimental kinetic analysis was performed for human CE-1-catalyzed cocaine hydrolysis. For CE-1-catalyzed cocaine hydrolysis, the computationally predicted free energy barrier (20.1 kcal/mol) is reasonably close to the experimentally derived turnover number (k_{cat} = 0.058 min^{-1}), indicating the reasonability of the computational results. The obtained novel mechanistic insights are expected to benefit not only CE-1 related rational drug discovery but also future research on the catalytic mechanism of other esterases.

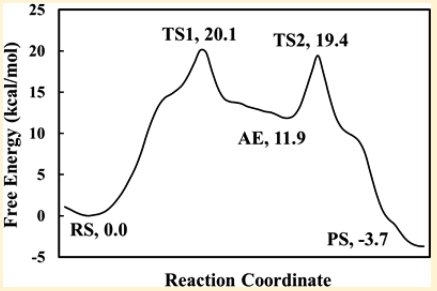

KEYWORDS: *enzyme, hydrolysis, drug metabolism, prodrug activation, drug inactivation*

INTRODUCTION

Carboxylesterases (CEs), ubiquitously expressed from bacteria to humans, represent a variety of esterases with comparable sequences and similar functions.[1] These esterases, spread all over the body, promiscuously catalyze a series of different reactions with various substrates, including hydrolysis of esters, thioesters, amides, and carbamates *etc.*[2] In particular, CE-1 is one of the promiscuous hydrolases, and it plays a leading role[3] in the human liver, serving as a crucial mediator of drug metabolism, activation, and inactivation processes. In fact, CE-1 is known as the crucial enzyme taking part in the metabolism of endogenous biomolecules and xenobiotics, including abused drugs, and important therapeutic agents.[3] For example, many prescription drugs, such as those for the treatment of congestive heart failure, diabetes, hypertension, and other polyfactorial diseases, contain the hydrolyzable functional groups and are substrates of CE-1.[3] Most prodrugs must be activated through hydrolysis to release the active drugs, and CE-1 activates a variety of prodrugs, such as oseltamivir, dabigatran etexilate, and mycophenolate mofetil.[3,4] Through catalytic hydrolysis, CE-1 also helps to inhibit angiotensin-converting enzyme (ACE) by activation of a variety of inhibitors, such as quinapril, benazepril, imidapril, and trandolapril.[3] Further, through catalyzing hydrolysis reactions, CE-1 inactivates a variety of drugs with hydrolyzable functional groups, such as methylphenidate, pethidine, clopidogrel, rufinamide, and oxybutynin.[5−8]

In addition to the above-mentioned primary biological role of CE-1 in metabolism/activation/inactivation of various xenobiotics (including clinically used drugs, prodrugs, abused drugs, and organophosphorus nerve agents *etc.*), CE-1 also plays roles in various other biological processes, *e.g.* managing the esterification levels of cholesterol and hydrolysis of esters of fatty acid.[3] With all of the important biological roles, it has been recognized that CE-1 may have potential to be a drug target, as well as functioning as a drug itself. To use CE-1 itself as a drug, it might be necessary to design a CE-1 mutant which improved enzyme function, stability, and selectivity for specific substrate(s), as we previously did in engineering other

Received: April 3, 2018
Revised: July 21, 2018
Accepted: July 26, 2018
Published: August 10, 2018

DOI: 10.1021/acs.molpharmaceut.8b00354
Mol. Pharmaceutics 2018, 15, 3871−3880

esterases for detoxification of cocaine by hydrolyzing it at the benzoyl ester group and its toxic metabolites.[9−23] For rational design of a drug targeting CE-1, it would also be helpful to understand the detailed functional role with respect to how CE-1 processes a substrate including the chemical transformation after the enzyme−substrate binding. So, it is crucial to know the fundamental catalytic mechanism of CE-1 against a typical substrate for understanding the detailed molecular mechanisms underlying the relevant biological roles of CE-1 and for future rational drug design in various kinds of therapeutic areas.

Of the known numerous substrates of CE-1, we are particularly interested in cocaine due to our continuing interest in rational design, discovery, and development of therapeutic enzymes for cocaine detoxification and medications. Cocaine is metabolized via three metabolic pathways, resulting in different metabolites. For benzoyl ester hydrolysis of cocaine, the reaction products are benzoic acid and ecgonine methyl ester (EME), whereas methanol and benzoylecgonine are the products for methyl ester hydrolysis. Cocaine oxidation leads to generation of norcocaine. The primary enzyme responsible for the benzoyl ester hydrolysis of cocaine is butyrylcholinesterase (BChE) in plasma, whereas CE-1 is responsible for the methyl ester hydrolysis of cocaine. The generation of norcocaine by oxidation of cocaine is catalyzed by liver cytochrome P450 3A4.[22,23] A detailed understanding of the BChE catalyzed fundamental reaction pathway for cocaine hydrolysis happening at the benzoyl ester group has led to successful design, discovery, and development of promising candidates of novel enzyme therapies under clinical development.[9,12,17,21,24−26] According to recently reported preclinical and clinical studies,[21,24,25] the cocaine methyl ester group related hydrolysis, catalyzed by CE-1, is the primary cocaine metabolic pathway in rats and humans.

The present study first aimed to understand the fundamental catalytic mechanism for hydrolysis occurring at the methyl ester group in CE-1-cocaine Michaelis−Menten complex by extensive simulations based on hybrid quantum mechanical/molecular mechanical (QM/MM) methodology, including molecular dynamics (MD) simulations, reaction-coordinate calculations, as well as the free energy simulations. Based on the results of simulations and calculations, CE-1-catalyzed cocaine methyl ester hydrolysis occurs through a unique pathway. As distinct from the classical reaction pathway of serine esterases, the enzymatic hydrolysis process by CE-1 particularly consists of a single-step acylation stage and a first discovered one-step deacylation stage. The deacylation occurs in only a single step without the traditional tetrahedral intermediate existing in numerous deacylation reactions of other esterases. In addition, an NH group of the substrate (cocaine) itself joins the oxyanion hole to stabilize the negatively charged carbonyl oxygen atom of the substrate in the transition states of both acylation and deacylation stages. Further, *in vitro* experimental kinetic analysis was performed for human CE-1-catalyzed cocaine hydrolysis. The computationally predicted free energy barrier (20.1 kcal/mol) of the rate-limiting acylation process is in good agreement with the experimentally determined kinetic data. The obtained mechanistic insights are expected to benefit not only CE-1 related rational drug discovery but also future research on the catalytic mechanism of other esterases.

METHODS

Computational Methods. *CE-1−Cocaine Complex Construction.* The initial three-dimensional coordinates of CE-1-cocaine complex were read from the crystallographic structure (PDB ID: 1MX5) in which a cocaine analog (homatropine) interacts with the active site of CE-1.[27] The cocaine was created by modification of homatropine. The CHARMM HBUILD module[28] was applied to add hydrogen atoms to protein, while hydrogen atoms of cocaine were added manually. The protonation states of all amino acids (that are acidic or basic under pH 7.4) were chosen based on the hydrogen bonding interaction between residues. The Ser221 oxygen (O^{γ}) atom was chosen as the center of the CE-1−cocaine complex. A 22 Å-radius water droplet was superimposed at the center of the CE-1−cocaine complex for the solvation purpose. All solvation and crystal water molecules were described by a modified TIP3P water model.[29,30] As shown in Figure S4, the atoms included in the QM region are the substrate (cocaine) and Ser221, Glu354, and His468 side chains of CE-1. Other atoms of the whole system are in the MM region. In addition, to model the deacylation process, methanol (a product of the acylation reaction) was deleted and replaced by a water molecule in the QM region. The boundaries between QM and MM regions were treated by link-atoms with the divided frontier charge (DIV) scheme.[31,32] The SCC-DFTB method implemented in CHARMM[33] and the all-hydrogen CHARMM potential function (PARAM27)[34] were applied for the QM and MM atoms, respectively. The nonbonded interactions between QM and MM atoms were calculated without truncation cutoff, while the truncation cutoff was 13 Å within the atoms of the MM region.

The stochastic boundary condition[35] was used for the MD simulation with the Ser221 oxygen (O^{γ}) atom as the center. The reaction region was within 20 Å from the center, and the buffer region included the atoms from 20 to 22 Å. The Newtonian and Langevin equations-of-motion were solved for reaction and buffer regions, respectively. The Langevin thermostat was used and the temperature bath was at 300 K. All other atoms locating outside of the reaction and buffer regions were frozen during all simulations. The SHAKE algorithm[36] was used to constrain the H atoms involving covalent bonds. The whole system was minimized first by the steepest descent (SD) method and then by the adopted-basis Newton−Raphson (ABNR) method. The heating process (from 50 to 298.15 K) was performed in 100 ps, followed by a 1.0 ns production run. The 1 fs time step was used for MD simulation.

QM/MM Reaction-Coordinate Calculations. The reaction-coordinate calculations were started from the last snapshot of the production run at various QM/MM levels. Semiempirical SCC-DFTB based QM/MM(SCC-DFTB:CHARMM27) reaction-coordinate calculations were carried out first, followed by density functional theory (DFT) based QM/MM(B3LYP/6-31G*:CHARMM27) reaction-coordinate calculations performed by CHARMM interfaced with the GAMESS-US program[37] for validation purposes and subsequent single-point energy calculations by CHARMM interfaced with the QChem program[38] at three different high level DFT based QM/MM methods, including QM/MM(B97-3/6-31G*:CHARMM27), QM/MM(B3LYP/6-311++G**:CHARMM27), and QM/MM(ωM06-D3/6-31G*:CHARMM27). The validation of the reaction-coordi-

DOI: 10.1021/acs.molpharmaceut.8b00354
Mol. Pharmaceutics 2018, 15, 3871−3880

nate calculations had been proved by a variety of previous similar and successful calculations on different BChE-catalyzed reactions.[17,39−48] All QM/MM reaction-coordinate calculations were performed to generate the potential energy surface along the reaction coordinates (RC) with the following protocol. The constrained ABNR minimizations were performed for each step along the RC (0.2 Å increase) for both acylation (from RS to AE) and deacylation (from AE to PS) processes. The force constant of the harmonic constraint is 10,000 kcal mol^{-1} $Å^{-2}$. Then similar calculations were performed backward from PS to AE (deacylation) and from AE to RS (acylation) along the same RC with a 0.2 Å decrease for each step. Finally, the forward and backward protocol was repeated to generate the potential energy surface along the RC.

To further confirm the single step mechanism for both acylation and deacylation processes, we performed the intrinsic reaction coordinate (IRC) calculations starting from the first-order saddle points (*e.g.* TS1 and TS2 geometries) at the QM/MM(SCC-DFTB:CHARMM27) level in order to check whether TS1 of acylation or TS2 of deacylation are the only TS between the RS and AE or between AE and PS, respectively.

Free Energy (Potential of Mean Force, PMF) Simulation. After the MD simulations at the QM/MM(SCC-DFTB:CHARMM27) level, the same-level PMF free energy simulation was performed using the umbrella sampling method,[52] and the free energy maps as a function of the RC were calculated by the Weighted Histogram Analysis Method (WHAM).[53] For both the acylation and deacylation processes, we first generated the potential energy maps along the respective RCs by adiabatic mapping calculations at the QM/MM(SCC-DFTB:CHARMM27) level. In order to characterize both the acylation and deacylation processes by free energy maps, PMF simulations were carried out with 80 windows. For each of the windows, 50 ps MD simulation was performed for equilibration, and a 50 ps production run was followed. One snapshot was saved every 0.5 ps. So, a total of 100 snapshots were saved per window. The harmonic biasing potential with a force constant of 150 kcal mol^{-1} $Å^{-2}$ was applied to PMF simulations.

Experimental Materials and Methods. *Construction of Eukaryotic Expression Plasmids.* Sources of materials are provided as part of the Supporting Information. Plasmid (pCMV-CE-1), constructed by using Gibson Assembly Master Mix, contains a sequence encoding native CE-1 followed by a 10× His Tag. Forward (5′-TTG GGA TTC GAA CAT CGA TTG AAT TCA TGT GGC TCC GTG CCT TTA TCC-3′) and reverse (5′-GTC ACA GGG ATG CCA CCC GTA GAT CTT CAG TGA TGG TGA TGA TGG TGG TGA TGA TGG TGC AGC TCT ATG TGT TCT GTC TG-3′) primers were designed to introduce a sequence encoding C-terminal 10× His Tag, and an overlap sequence of vector at each end of the PCR product. The cDNA encoding CE-1 was amplified by PCR using the plasmid (clone ID: HsCD00338654) as a template. Linearized pCMV-MCS vector was prepared by restriction digestion using restriction enzymes EcoR I and *Bgl*II. Both PCR-amplified DNA fragment and restriction enzyme-digested vector were purified by the QIAquick Gel Extraction Kit. Purified PCR-amplified DNA fragment was ligated into pCMV-MCS using Gibson Assembly Master Mix.

Expression and Purification of CE-1. The CHO-S cell incubation was carried out in humidified atmosphere with 8% CO_2, and the environmental temperature was 37 °C. The TransIT-PRO transfection kit was applied for transfection of CHO-S cells with pCMV-CE-1 plasmid. The required cell density for transfection is around 1.0×10^6 cells/mL. After 7 days, culture medium containing secreted CE-1 in Gibco FreeStyle CHO expression medium with 8 mM glutamine was harvested by a centrifugation (4,000*g* and 20 min) for removal of CHO-S cells. Then, the His-tag affinity chromatography was applied for protein (CE-1) purification purpose with the following protocol. Briefly, cell free culture medium with His-tag CE-1 was mixed with pre-equilibrated nickel NTA agarose for 1 h, and the mixture was stirred occasionally. Then, the column washing with 20 mM Tris·HCl was carried out at pH 7.4, and stopped once the OD_{280} was less than 0.02. Finally, the elution of CE-1 by imidazole was performed with a gradient from 0 to 500 mM. Before use, the purified protein was stored at 4 °C, after a dialysis process with a buffer (1 M glycine, 20% Sorbitol, 50 mM HPEPS) at pH 7.4.

Enzyme Activity Assay. The enzymatic reaction with a total volume 200 μL was initialed by adding the enzyme (CE-1) solution and was stopped through denaturing the enzyme by considerably decreasing the pH of the enzyme solution with 200 μL of 200 mM HCl. The sample was then centrifuged at 13,200 rpm for 10 min to precipitate the denatured protein, and 100 μL of supernatant was vortex mixed for 15 s with 100 μL of 0.1 μM benzoylecgonine-D3 solution (internal standard, IS) in a clean tube, followed by a 10 min centrifugation at 13,200 rpm. Finally, the supernatant was analyzed by a LC-MS/MS method according to the procedure established in our previous study.[54]

RESULTS AND DISCUSSION

CE-1−Cocaine Binding Mode. It has been known that CE-1 is one of the enzymes belonging to the *α/β* fold family of hydrolases,[55] characterized by a classic catalytic triad and an oxyanion hole. The average structure of the Michalis−Menten complex obtained from the simulation at the QM/MM(SCC-DFTB:CHARMM27) level revealed that (−)-cocaine (the naturally occurring and biologically active enantiomer of cocaine) occupies the active site of human CE-1 very well. Similar to other hydrolases in the *α/β* fold hydrolase family, the residues of catalytic triad (i.e., Ser221, Glu354, and His467) and oxyanion hole are located in the active site of CE-1. The oxyanion hole was formed by the backbone amide (NH) groups from the residues Gly143, Gly142, and Ala222. According to the average structure (see Figure S1 of Supporting Information), the distance between the Ser221 side chain hydroxyl oxygen of CE-1 and the methyl ester group carbonyl carbon of (−)-cocaine is 2.93 Å. This good alignment implicates for the upcoming nucleophilic attack. On the contrary, alignment between the oxyanion hole and the methyl ester group carbonyl carbon of cocaine is imperfect, and no hydrogen bond was found between the enzyme and substrate. Interestingly, an intramolecular hydrogen bond was found between the NH group and the carbonyl oxygen of the reactive methyl ester group of cocaine. Such an intramolecular hydrogen bond may also join the oxyanion hole to stabilize the transition states during the acylation and deacylation processes like the substrate-assisted oxyanion hole stabilization.[56] Besides the residues of catalytic triad and oxyanion hole, CE-1 forms a mainly hydrophobic pocket to interact with cocaine, including a series of hydrophobic residues, as shown in Figure S1.

DOI: 10.1021/acs.molpharmaceut.8b00354
Mol. Pharmaceutics 2018, 15, 3871−3880

Reaction Pathway of Acylation. Using the Michalis−Menten complex (reactant state, RS, depicted in Figure 1) as

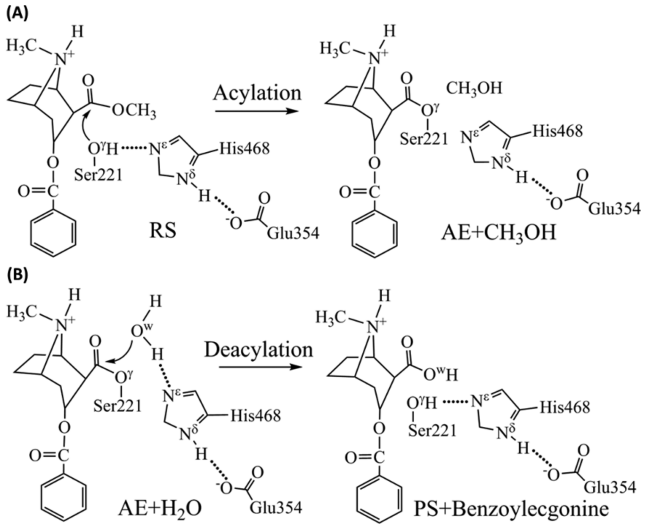

Figure 1. Reaction pathways for human CE-1-catalyzed hydrolysis of (−)-cocaine. (A) Acylation process without existence of a tetrahedral intermediate: Reactant State (RS), and Acyl-Enzyme (AE) + Methanol (CH_3OH). (B) Deacylation process without existence of a tetrahedral intermediate: Acyl-Enzyme (AE) + H_2O, and Product State (PS).

the starting point, the QM/MM(SCC-DFTB:CHARMM27) and QM/MM(B3LYP/6-31G*:CHARMM27) reaction-coordinate calculations were carried out and followed by single-point energy calculations at the QM/MM(ωB97X-D3/6-311++G**:CHARMM27), QM/MM(ωM06-D3/6-311++G**:CHARMM27), and QM/MM(B3LYP/6-311++G**:CHARMM27) levels. Based on the calculations at various QM/MM levels as shown in Figures 2 and S3, the acylation of CE-1 with (−)-cocaine is a reaction process happening in a single step. The acylation process happens along with a new covalent bond (C−O^{γ}) forming and a covalent bond (C−O) breaking. During the process, the Ser221 hydroxyl oxygen (O^{γ}) atom moves close to the carbonyl carbon (C) atom of cocaine until a covalent bond is formed. At the same time, the cocaine methyl ester oxygen (O) atom moves away from the cocaine carbonyl carbon (C) atom, resulting in breaking of the covalent bond (C−O). To cover the bond forming and breaking processes in the reaction-coordinate calculations, two covalent bond lengths were combined linearly to generate the reaction coordinate (RC) 1, *i.e,* RC1 = r(C−O) − r(C−O^{γ}). Moreover, the intrinsic reaction coordinate (IRC) calculation was carried out using the optimized transition state (TS1) structure as a starting point at the QM/MM(SCC-DFTB:CHARMM27) level. As a result of the IRC calculations, TS1 moved forward and backward smoothly toward AE and RS, respectively. The results of the IRC calculations support the conclusion made by the reaction-coordinate calculations that only one transition state was contained in the acylation process.

As revealed by the QM/MM reaction-coordinate and IRC calculations, only one transition state was detected in the acylation process (TS1 depicted in Figure 2C) between the RS (Figure 2B) and AE structures, resulting in a one-step reaction process in which the bond r(C−O^{γ}) forming by nucleophilic attack and the bond r(C−O) breaking happened simultaneously. Meanwhile, the Ser221 side chain hydroxyl hydrogen atom (H^{γ}) moves away from O^{γ} and approaches the O atom of the cocaine gradually. As seen in Figure 2E, the r(O−H^{γ}), representing the O−H^{γ} distance, gets shorter gradually. Meanwhile, the r(N^{ϵ}−H^{γ}), representing the N^{ϵ}−H^{γ} distance, gets shorter until reaching TS1 and then gets longer from TS1 to AE. In the acylation process, the shortest r(N^{ϵ}−H^{γ}) is around 1.08 Å, very close to the length of a typical N−H covalent bond. When r(N^{ϵ}−H^{γ}) becomes the shortest (∼1.08 Å), the r(C−O) and r(C−O^{γ}) become ∼1.51 Å and ∼1.86 Å, respectively. Clearly, no covalent bond is formed between C atom and oxygen atoms (O and O^{γ}). Hence, one may reasonably say that H^{γ} first transfers to N^{ϵ} and then immediately transfers to O during the single-step acylation process. As a result, the acylation process involves one and only TS1 that contains a partially broken C−O bond and an unformed O−H^{γ} bond, as seen in Figure 2C and E. Therefore, one may also reasonably say that all aforementioned bond forming (e.g., the nucleophilic attack) and breaking (e.g., C−O bond breaking) processes are involved in a concerted acylation process (depicted in Figure 2D) producing the acylated enzyme AE. Such a concerted single-step acylation process has only been observed recently for BChE-catalyzed hydrolysis of "hunger hormone" ghrelin.[4851] Observably, the newly defined concerted single-step acylation process and traditional two-step acylation process are entirely distinct reaction mechanisms.

Based on the single-step reaction pathway, the hydrogen bond (O···H) distance formed between the cocaine methyl ester group O atom and the Ala222 amide group becomes significantly shorter in TS1 compared to RS, as shown in Figure 2B and C. This enhanced hydrogen bonding together with the aforementioned intramolecular hydrogen bonding help to stabilize the negative charge of TS1. Additionally, no proton transfer was detected between the side chains of His467 and Glu354 in the acylation process.

In order to determine the free energy for the acylation process, the dynamics of the reaction process was simulated by MD based potential of mean force (PMF) calculations at the QM/MM(SCC-DFTB:CHARMM27) level. As a result of the PMF simulations, the free energy maps were plotted in Figure 2. As shown in Figure 4, the obtained free energy map shows the similar trend with reaction-coordinate calculation derived potential energy maps of the acylation process. Again, the preassumed traditional tetrahedral intermediate TI_a was not found in the acylation process, because no local energy minimum was shown on the free energy map. Only one saddle point existed in the free energy maps, supporting the finding of one-step acylation process of CE-1 with cocaine.

Reaction Pathway of Deacylation. The deacylation process of human CE-1 with (−)-cocaine was studied using the same computational methods as used for the acylation process, such as the reaction-coordinate calculations and single point energy calculations at different QM/MM levels, starting from the AE structure. As shown in Figures 3 and S3, all QM/MM calculations consisting of various methods at various QM/MM levels show that the deacylation process of acylated human CE-1 with cocaine is a one-step process, as well. The deacylation process happens along with a new covalent bond (C−O^{w}) forming and a covalent bond (C−O^{γ}) breaking. During the process, the water oxygen (O^{w}) atom moves close to the carbonyl carbon (C) atom of cocaine until a covalent bond formed. At the same time, the hydroxyl oxygen (O^{γ}) of the Ser221 side chain moves away from the cocaine carbonyl

DOI: 10.1021/acs.molpharmaceut.8b00354
Mol. Pharmaceutics 2018, 15, 3871−3880

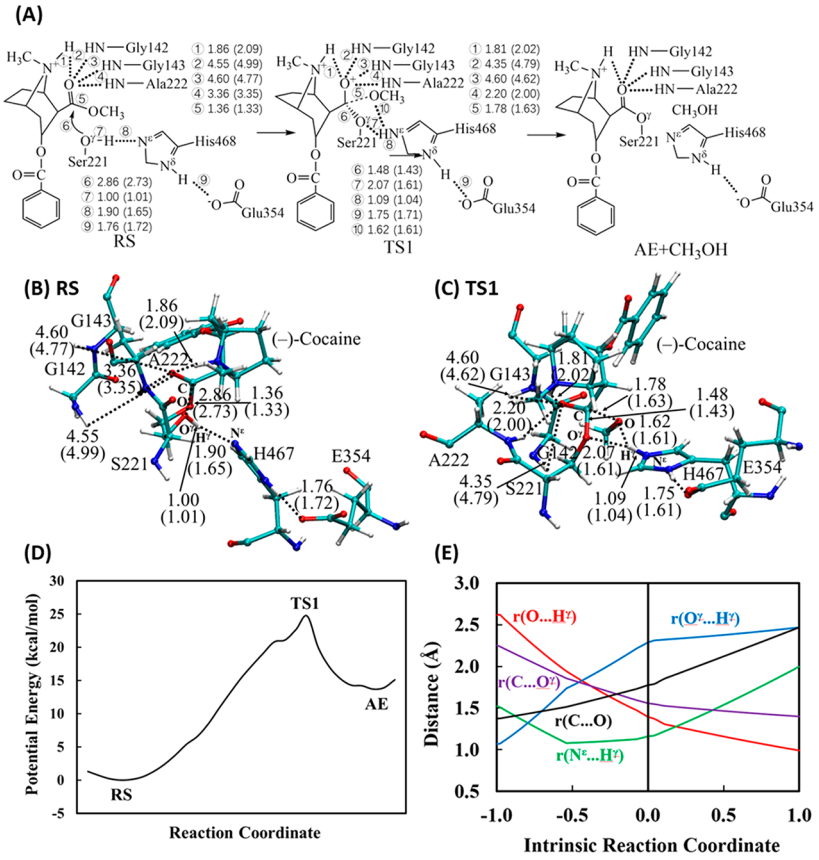

Figure 2. (A) Acylation reaction pathway for human CE-1 catalyzed hydrolysis of (−)-cocaine. Optimized geometries of (B) the reactant state (RS) and (C) the transition state (TS1) for the acylation process of human CE-1-catalyzed hydrolysis of (−)-cocaine. Indicated in the figures are the internuclear distances (Å) optimized at the QM/MM(SCC-DFTB:CHARMM27) level, and the values in parentheses refer to the distances optimized at the QM/MM(B3LYP/6-31G*:CHARMM27) level. (D) Plot of the potential energy vs the reaction coordinate (RC1) used in the QM/MM(SCC-DFTB:CHARMM27) reaction-coordinate calculations; RC1 = r(C−O) − r(C−O$^{\gamma}$). (E) Plots of key internuclear distances vs the intrinsic reaction coordinate (IRC) calculations at the QM/MM(SCC-DFTB:CHARMM27) level. The distances shown include the following atoms: C (carbonyl carbon atom on the methyl ester of cocaine); O (ester oxygen atom on the methyl ester of cocaine); O$^{\gamma}$ (hydroxyl oxygen atom on the Ser221 side chain of CE-1; H$^{\gamma}$ (hydroxyl hydrogen on the Ser221 side chain of CE-1); and N$^{\varepsilon}$ (nitrogen atom on the His438 side chain of CE-1).

carbon (C) atom, resulting in breaking of the covalent bond (C−O). To cover the bond forming and breaking in the deacylation process by QM/MM reaction-coordinate calculations, two covalent bond lengths were combined linearly to generate the reaction coordinate (RC) 2, *i.e.,* RC2 = r(C−O$^{\gamma}$) − r(C−O^{w}). Moreover, the intrinsic reaction coordinate (IRC) calculation was carried out using the optimized transition state (TS2) structure as a starting point at the QM/MM(SCC-DFTB:CHARMM27) level. According to the IRC calculation, TS2 moved forward and backward smoothly toward the product state (PS) and AE, respectively. The data obtained from the IRC calculations support the conclusion made by the reaction-coordinate calculations that only one transition state was contained in the deacylation process.

As revealed by the QM/MM reaction-coordinate and IRC calculations, only one transition state was detected in the deacylation process (TS2 depicted in Figure 3C) between the AE (Figure 3B) and PS structures, resulting in a one-step reaction process in which the bond r(C−O^{w}) forming by nucleophilic attack and the bond r(C−O$^{\gamma}$) breaking happened simultaneously. Meanwhile, the water hydrogen atom (H^{w}) moves away from O^{w} and approaches the O$^{\gamma}$ atom of the Ser221 gradually. As seen in Figure 3E, the r(O$^{\gamma}$−H^{w}), representing the O$^{\gamma}$−H^{w} distance, gets shorter gradually. Meanwhile, the r(N$^{\varepsilon}$−H^{w}), representing the N$^{\varepsilon}$−H^{w} distance, gets shorter until reaching TS2 and then gets longer from TS2 to PS. In the acylation process, the shortest r(N$^{\varepsilon}$−H$^{\gamma}$) is around 1.08 Å, very close to the length of a typical N−H covalent bond. When r(N$^{\varepsilon}$−H$^{\gamma}$) is the shortest (∼1.08 Å), the r(C−O^{w}) and r(C−O$^{\gamma}$) are ∼1.79 Å and ∼1.43 Å, respectively. Clearly, no covalent bond is formed between the C atom and the oxygen atoms (O^{w} and O$^{\gamma}$). Hence, one may reasonably say that H^{w} first transfers to N$^{\varepsilon}$ and then immediately transfers to O$^{\gamma}$ during the single-step deacylation process. As a result, the deacylation process involves one and only TS2 that contains a partially broken C−O$^{\gamma}$ bond and an unformed O$^{\gamma}$−H^{w} bond, as seen in Figures 3C and E. Therefore, one may also reasonably say that all aforementioned bond forming (e.g., the nucleophilic attack) and breaking (e.g., C−O$^{\gamma}$ bond breaking) processes are involved in a concerted deacylation process (depicted in Figure 3D) producing the product in the PS. Observably, the newly defined concerted single-step acylation process and traditional two-step acylation process are entirely distinct reaction mechanisms. Such a concerted single-step deacylation process has never been reported.

Based on the novel single-step reaction pathway, the hydrogen bond (O···H) distance formed between cocaine methyl ester group O atom and Ala222 amide group becomes

DOI: 10.1021/acs.molpharmaceut.8b00354
Mol. Pharmaceutics 2018, 15, 3871−3880

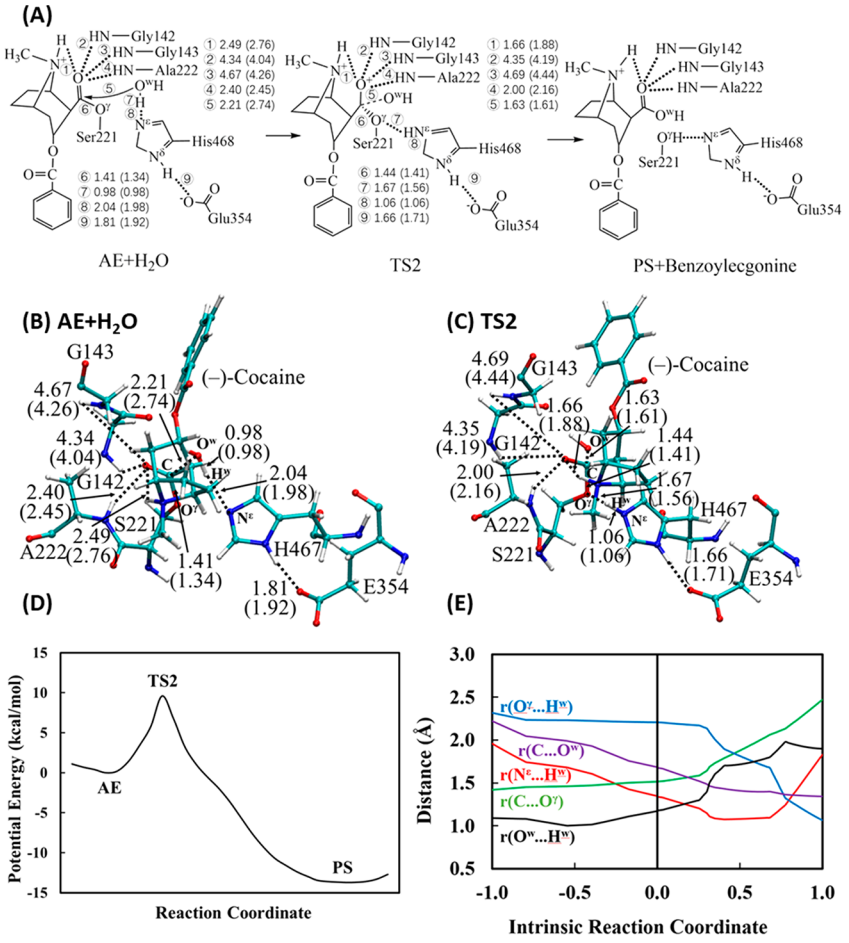

Figure 3. (A) Deacylation reaction pathway for human CE-1 catalyzed hydrolysis of (−)-cocaine. Optimized geometries of (B) the acyl-enzyme (AE) and (C) the transition state (TS2) for the deacylation process of human CE-1-catalyzed hydrolysis of (−)-cocaine. Indicated in the figures are the internuclear distances (Å) optimized at the QM/MM(SCC-DFTB:CHARMM27) level, and the values in parentheses refer to the distances optimized at the QM/MM(B3LYP/6-31G*:CHARMM27) level. (D) Plot of the potential energy vs the reaction coordinate (RC2) used in the QM/MM(SCC-DFTB:CHARMM27) reaction-coordinate calculations; RC1 = r(C−O^{γ}) − r(C−O^{w}). (E) Plots of key internuclear distances vs the intrinsic reaction coordinate (IRC) calculations at the QM/MM(SCC-DFTB:CHARMM27) level. The distances shown include the following atoms: C (carbonyl carbon atom on the methyl ester of cocaine); O^{w} (water oxygen atom); H^{w} (water hydrogen atom); O^{γ} (hydroxyl oxygen atom on the Ser221 side chain of CE-1; and N^{ε} (nitrogen atom on the His438 side chain of CE-1).

significantly shorter in TS2 compared to AE, as shown in Figures 3B and C. This enhanced hydrogen bonding together with the aforementioned intramolecular hydrogen bonding help to stabilize the negative charge of TS2. Additionally, no proton transfer was found between the side chains of His467 and Glu354 in the deacylation process.

In order to determine the free energy for the deacylation process, the dynamics of the reaction process was simulated by MD based PMF calculations at the QM/MM(SCC-DFTB:CHARMM27) level. As a result of the PMF simulations, the free energy maps along RC2 were plotted in Figure 3. As shown in Figure 4, the obtained free energy map shows the similar trend with reaction-coordinate calculation derived potential energy maps of the deacylation process. Again, the preassumed traditional tetrahedral intermediate TI_a was not found in the deacylation process, because no local energy minimum was shown in the free energy map between AE and PS. Only one saddle point exists in the free energy maps, supporting the finding of the one-step acylation process of CE-1 with cocaine.

Calculated Free Energy Profile and Available Experimental Kinetic Data. The free energy profile depicted in

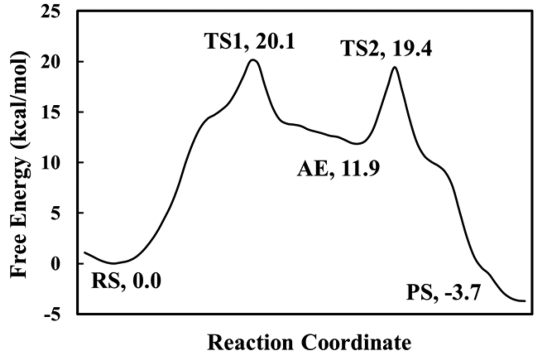

Figure 4. Free energy profile determined by the QM/MM(SCC-DFTB:CHARMM27) calculations based on PMF free energy maps for the entire reaction process (acylation and deacylation) of human CE-1-catalyzed hydrolysis of (−)-cocaine.

Figure 4 was plotted by combination of the acylation and deacylation free energy maps calculated for CE-1-catalyzed (−)-cocaine hydrolysis. According to Figure 4, the entire CE-1-catalyzed (−)-cocaine hydrolysis process on one hand contains RS, AE, and PS, which is consistent with the

DOI: 10.1021/acs.molpharmaceut.8b00354
Mol. Pharmaceutics 2018, 15, 3871−3880

traditional reaction processes catalyzed by numerous serine esterases. On the other hand, the hydrolysis process happening in the CE-1-cocaine complex contains only two TSs without any TI, which is observably different from the usually assumed esterase reaction pathway involving four TSs and two TIs. The TS1 of the acylation process is the rate-limiting transition state with a free energy barrier of 20.1 kcal/mol being higher than the free energy barrier (19.4 kcal/mol) associated with TS2. The rate-limiting free energy barrier (20.1 kcal/mol) for CE-1-catalyzed (−)-cocaine methyl ester hydrolysis is ∼1 kcal/mol higher compared to ∼19 kcal/mol (derived from the experimental k_{cat} of 4.1 min^{-1})[12] known for (−)-cocaine benzoyl ester hydrolysis catalyzed by BChE, predicting a rather low k_{cat} for CE-1-catalyzed (−)-cocaine hydrolysis.

Experimental Kinetic Analysis. The calculated free energy profile discussed above predicted that the turnover number (k_{cat}) for CE-1-catalyzed (−)-cocaine methyl ester hydrolysis should be significantly lower than that for (−)-cocaine hydrolysis at the benzoyl ester group catalyzed by CE-1. This sounds surprising, because it has been reported that the primary metabolic pathway of (−)-cocaine in rats and humans is the (−)-cocaine methyl ester hydrolysis (catalyzed by CE-1), as evidenced from reported *in vivo* cocaine pharmacokinetic data.[21,24,25] According to the reported *in vivo* cocaine pharmacokinetic data, the overall CE-1-catalyzed (−)-cocaine hydrolysis (methyl ester) reaction should be more efficient than BChE-catalyzed (−)-cocaine hydrolysis (benzoyl ester) in the human body. The faster (−)-cocaine methyl ester hydrolysis by CE-1 could be due to the higher catalytic efficiency of the endogenous metabolic enzyme CE-1 compared to the endogenous enzyme BChE or the enzyme CE-1 being much more abundant than BChE in the body or both. So, it is crucial to know the actual kinetic parameters (k_{cat} and K_M) of CE-1-catalyzed (−)-cocaine methyl ester hydrolysis for examining/validating the computational prediction and further understanding why CE-1-catalyzed (−)-cocaine methyl ester hydrolysis is the primary metabolic pathway of (−)-cocaine *in vivo*.

CE-1 has been characterized previously for its kinetic parameters (k_{cat} and K_M) against many substrates. However, previously reported kinetic characterization of CE-1-catalyzed (−)-cocaine methyl ester hydrolysis has been incomplete. Only K_M was determined to be 0.12 mM (or 120 μM)[5,57,58] by the kinetic analysis using CE-1 protein extracted from human tissues. To the best of our knowledge, we are not aware of a reported k_{cat} value for CE-1-catalyzed (−)-cocaine hydrolysis, although a report by Zhang et al.[5] (who measured the catalytic parameters of CE-1 against other substrates) listed a k_{cat}/K_M value (0.5 mM^{-1} min^{-1}) obtained from a report by Pindel et al.[58] Actually, the report by Pindel et al.[58] indicated that the K_M of 0.12 mM was obtained from an earlier report[57] and that "the k_{cat}/K_M was not determined."[58] Without knowing the k_{cat} value, we carried out a kinetic analysis of CE-1-catalyzed (−)-cocaine methyl ester hydrolysis. The obtained kinetic data are depicted in Figure 5, showing that k_{cat} = 0.058 min^{-1} and K_M = 4.3 μM.

Notably, our experimental K_M value of 4.3 μM is much smaller than the earlier K_M value of 120 μM reported by Brzezinski et al.[57] and cited by Pindel et al.[58] and Zhang et al.[5] The huge difference in the experimental K_M was likely due to the difference existing in the CE-1 protein preparation process. Generally speaking, a protein (particularly that from a stored human tissue) could become partially inactive (in terms of the binding affinity and activity) during the complicated collection,

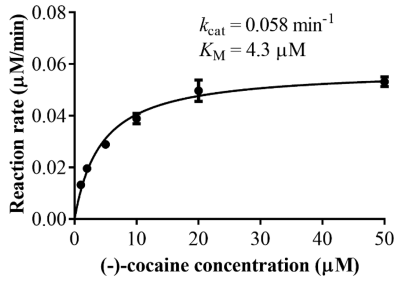

Figure 5. Kinetic data obtained *in vitro* for (−)-cocaine methyl ester hydrolysis catalyzed by human CE-1, showing that k_{cat} = 0.058 min^{-1}, K_M = 4.3 μM, and k_{cat}/K_M = 1.35 × 10^4 min^{-1} M^{-1}. The reaction rate is represented in μM min^{-1} per μM enzyme (CE-1).

treatment, storage, and extraction processes. Whereas the kinetic analysis by Brzezinski et al.[57] was based on the use of human tissue extracts, our kinetic analysis was based on the freshly expressed and purified CE-1 protein in readily controlled experimental conditions. In addition, the protein sample used in our kinetic characterization revealed a higher binding affinity (reflected by the lower K_M). So, the catalytic parameters determined in the present study should be more reasonable.

The catalytic rate constant (k_{cat} = 0.058 min^{-1}) determined for CE-1-catalyzed (−)-cocaine hydrolysis (methyl ester) is much lower than that (k_{cat} = 4.1 min^{-1}) for BChE-catalyzed (−)-cocaine benzoyl ester hydrolysis,[59] although they have similar K_M values (4.3 μM for CE-1-catalyzed (−)-cocaine methyl ester hydrolysis and 4.5 μM for BChE-catalyzed (−)-cocaine benzoyl ester hydrolysis[59]). The catalytic efficiency (k_{cat}/K_M = 1.35 × 10^4 min^{-1} M^{-1}) obtained for CE-1-catalyzed (−)-cocaine hydrolysis (methyl ester) is ∼67-fold lower than that (k_{cat}/K_M = 9.1 × 10^5 min^{-1} M^{-1}) for BChE-catalyzed (−)-cocaine hydrolysis (benzoyl ester). Based on the comparison of the experimental catalytic parameters, in comparison with the (−)-cocaine hydrolysis (benzoyl ester) *in vivo*, the faster (−)-cocaine hydrolysis (methyl ester) *in vivo* is solely due to the high abundance of CE-1 in the body.[60]

According to the conventional transition state theory,[61] the experimentally derived free energy barrier of ∼21.5 kcal/mol was calculated based on the experimental turnover number (k_{cat} = 0.058 min^{-1}), for CE-1-catalyzed (−)-cocaine methyl ester hydrolysis. The computationally predicted and experimentally derived free energy barriers (20.1 kcal/mol vs ∼21.5 kcal/mol) are reasonably close to each other, indicating the reasonability of the novel mechanistic insights obtained by computational and experimental studies.

■ CONCLUSION

All of the computational data obtained from the QM/MM simulations, such as the MD, reaction-coordinate calculations, and PMF simulations, have been converging toward one conclusion that catalytic cocaine hydrolysis on the methyl ester group by CE-1 follows a novel reaction pathway consisting of only two reaction steps: a one-step acylation process and a one-step deacylation process. For the oxyanion hole stabilization in both processes, the NH group of the substrate (cocaine) joins the oxyanion hole to form an additional hydrogen bond with the oxygen of the substrate methyl ester carbonyl group in the transition states. Thus, the transition states are stabilized by both intermolecular and intramolecular hydrogen bonds with the oxygen of the substrate methyl ester

DOI: 10.1021/acs.molpharmaceut.8b00354
Mol. Pharmaceutics 2018, 15, 3871−3880

carbonyl group. The rate-determining step for the enzymatic hydrolysis of cocaine by CE-1 is the one-step acylation process, with the free energy barrier predicted to be 20.1 kcal/mol.

Further, our *in vitro* experimental kinetic study has shown that k_{cat} = 0.058 min^{-1} and K_M = 4.3 μM. The turnover number (k_{cat} = 0.058 min^{-1}) determined for CE-1-catalyzed (−)-cocaine hydrolysis (methyl ester) is significantly less than that (k_{cat} = 4.1 min^{-1}) for BChE-catalyzed (−)-cocaine benzoyl ester hydrolysis. The catalytic efficiency (k_{cat}/K_M = 1.35 × 10^4 min^{-1} M^{-1}) obtained for CE-1-catalyzed (−)-cocaine hydrolysis (methyl ester) is ∼67-fold smaller than that (k_{cat}/K_M = 9.1 × 10^5 min^{-1} M^{-1}) for BChE-catalyzed (−)-cocaine hydrolysis (benzoyl ester), although the overall (−)-cocaine hydrolysis (methyl ester) *in vivo* is faster due to the fact that CE-1 is much more abundant in the body.

The computationally predicted and experimentally derived free energy barriers (20.1 kcal/mol vs ∼21.5 kcal/mol) are close to each other, suggesting that the obtained mechanistic insights are reasonable. The obtained novel mechanistic insights are expected to benefit not only CE-1 related rational drug discovery but also future research on catalytic mechanisms of other esterases.

■ ASSOCIATED CONTENT

Supporting Information

The Supporting Information is available free of charge on the ACS Publications website at DOI: 10.1021/acs.molpharmaceut.8b00354.

Additional Figures (S1 to 4) for the detailed computational data and additional computational and experimental details. (PDF)

■ AUTHOR INFORMATION

Corresponding Authors

*Phone: 859-218-2992. Fax: 859-257-7585. Email: fzhen2@uky.edu.

*Phone: 859-323-3943. Fax: 859-257-7585. E-mail: zhan@uky.edu.

ORCID

Chang-Guo Zhan: 0000-0002-4128-7269

Author Contributions

⊥J.Y. and X.C. contributed equally to this work.

Notes

The authors declare no competing financial interest.

■ ACKNOWLEDGMENTS

We thank the National Institutes of Health (NIH) for supporting this work through R01 grants (R01 DA025100, R01 DA013930, R01 DA032910, and R01 DA035552) and the NIDA Translational Avant-Garde Award (UH2/UH3 DA041115) and the National Science Foundation (NSF) through grant CHE-1111761. All of the computational and *in vitro* experiments were carried out at the University of Kentucky. The Computer Center at University of Kentucky is also thanked for providing a Dell X-series Cluster with 4,768 processors or 384 nodes and sufficient computing time.

■ REFERENCES

(1) Hatfield, M. J.; Wierdl, M.; Wadkins, R. M.; Potter, P. M. Modifications of human carboxylesterase for improved prodrug activation. *Expert Opin. Drug Metab. Toxicol.* **2008**, *4*, 1153−1165.

(2) Laizure, S. C.; Herring, V.; Hu, Z.; Witbrodt, K.; Parker, R. B. The Role of Human Carboxylesterases in Drug Metabolism: Have We Overlooked Their Importance? *Pharmacotherapy* **2013**, *33*, 210−222.

(3) Thomsen, R.; Rasmussen, H. B.; Linnet, K. *In Vitro* Drug Metabolism by Human Carboxylesterase 1: Focus on Angiotensin-Converting Enzyme Inhibitors. *Drug Metab. Dispos.* **2014**, *42*, 126−133.

(4) Hu, Z.-Y.; Parker, R. B.; Herring, V. L.; Laizure, S. C. Conventional liquid chromatography/triple quadrupole mass spectrometry based metabolite identification and semi-quantitative estimation approach in the investigation of in vitro dabigatran etexilate metabolism. *Anal. Bioanal. Chem.* **2013**, *405*, 1695−1704.

(5) Zhang, J.; Burnell, J. C.; Dumaual, N.; Bosron, W. F. Binding and hydrolysis of meperidine by human liver carboxylesterase hCE-1. *J. Pharmacol. Exp. Ther.* **1999**, *290*, 314−318.

(6) Sato, Y.; Miyashita, A.; Iwatsubo, T.; Usui, T. Conclusive identification of the oxybutyninhydrolyzing enzyme in human liver. *Drug Metab. Dispos.* **2012**, *40*, 902−906.

(7) Tang, M.; Mukundan, M.; Yang, J.; Charpentier, N.; LeCluyse, E. L.; Black, C.; Yang, D.; Shi, D.; Yan, B. Antiplatelet agents aspirin and clopidogrel are hydrolyzed by distinct carboxylesterases, and clopidogrel is transesterificated in the presence of ethyl alcohol. *J. Pharmacol. Exp. Ther.* **2006**, *319*, 1467−1476.

(8) Williams, E. T.; Carlson, J. E.; Lai, W. G.; Wong, Y. N.; Yoshimura, T.; Critchley, D. J.; Narurkar, M. Investigation of the metabolism of rufinamide and its interaction with valproate. *Drug Metab. Lett.* **2011**, *5*, 280−289.

(9) Pan, Y.; Gao, D.; Yang, W.; Cho, H.; Yang, G.; Tai, H.-H.; Zhan, C.-G. Computational redesign of human butyrylcholinesterase for anticocaine medication. *Proc. Natl. Acad. Sci. U. S. A.* **2005**, *102* (46), 16656−16661.

(10) Pan, Y.; Gao, D.; Yang, W.; Cho, H.; Zhan, C.-G. Free Energy Perturbation (FEP) Simulation on the Transition States of Cocaine Hydrolysis Catalyzed by Human Butyrylcholinesterase and Its Mutants. *J. Am. Chem. Soc.* **2007**, *129* (44), 13537−13543.

(11) Gao, D.; Cho, H.; Yang, W.; Pan, Y.; Yang, G.; Tai, H. H.; Zhan, C.-G. Computational Design of a Human Butyrylcholinesterase Mutant for Accelerating Cocaine Hydrolysis Based on the Transition-State Simulation. *Angew. Chem., Int. Ed.* **2006**, *45* (4), 653−657.

(12) Zheng, F.; Yang, W. C.; Ko, M. C.; Liu, J. J.; Cho, H.; Gao, D. Q.; Tong, M.; Tai, H. H.; Woods, J. H.; Zhan, C.-G. Most Efficient Cocaine Hydrolase Designed by Virtual Screening of Transition States. *J. Am. Chem. Soc.* **2008**, *130* (36), 12148−12155.

(13) Zheng, F.; Zhan, C.-G. Rational design of an enzyme mutant for anti-cocaine therapeutics. *J. Comput.-Aided Mol. Des.* **2008**, *22*, 661−671.

(14) Zheng, F.; Zhan, C.-G. Recent progress in protein drug design and discovery with a focus on novel approaches to the development of anti-cocaine medications. *Future Med. Chem.* **2009**, *1*, 515−528.

(15) Zheng, F.; Zhan, C.-G. Enzyme therapy approaches for treatment of drug overdose and addiction. *Future Med. Chem.* **2011**, *3*, 9−13.

(16) Zheng, F.; Zhan, C.-G. Are pharmacokinetic approaches feasible for treatment of cocaine addiction and overdose? *Future Med. Chem.* **2012**, *4*, 125−128.

(17) Zheng, F.; Xue, L.; Hou, S.; Liu, J.; Zhan, M.; Yang, W.; Zhan, C.-G. A highly efficient cocaine-detoxifying enzyme obtained by computational design. *Nat. Commun.* **2014**, *5*, 3457.

(18) Hou, S.; Xue, L.; Yang, W.; Fang, L.; Zheng, F.; Zhan, C.-G. Substrate selectivity of high-activity mutants of human butyrylcholinesterase. *Org. Biomol. Chem.* **2013**, *11*, 7477−7485.

(19) Gao, D.; Narasimhan, D. L.; Macdonald, J.; Ko, M.-C.; Landry, D. W.; Woods, J. H.; Sunahara, R. K.; Zhan, C.-G. Thermostable variants of cocaine esterase for long-time protection against cocaine toxicity. *Mol. Pharmacol.* **2009**, *75*, 318−323.

(20) Chen, X.; Xue, L.; Hou, S.; Jin, Z.; Zhang, T.; Zheng, F.; Zhan, C.-G. Long-acting cocaine hydrolase for addiction therapy. *Proc. Natl. Acad. Sci. U. S. A.* **2016**, *113*, 422−427.

DOI: 10.1021/acs.molpharmaceut.8b00354
Mol. Pharmaceutics 2018, 15, 3871−3880

(21) Zhang, T.; Zheng, X.; Zhou, Z.; Chen, X.; Jin, Z.; Deng, J.; Zhan, C.-G.; Zheng, F. Clinical potential of an enzyme-based novel therapy for cocaine overdose. *Sci. Rep.* **2017**, *7*, 15303.
(22) Zhan, M.; Hou, S.; Zhan, C.-G.; Zheng, F. Kinetic characterization of high-activity mutants of human butyrylcholinesterase for the cocaine metabolite norcocaine. *Biochem. J.* **2014**, *457*, 197−206.
(23) Hou, S.; Zhan, M.; Zheng, X.; Zhan, C.-G.; Zheng, F. Kinetic characterization of human butyrylcholinesterase mutants for hydrolysis of cocaethylene. *Biochem. J.* **2014**, *460*, 447−457.
(24) Zheng, X.; Zhou, Z.; Zhang, T.; Jin, Z.; Chen, X.; Deng, J.; Zhan, C.-G.; Zheng, F. Effectiveness of a cocaine hydrolase for cocaine toxicity treatment in male and female rats. *AAPS J.* **2018**, *20*, 3.
(25) Cohen-Barak, O.; Wildeman, J.; van de Wetering, J.; Hettinga, J.; Schuilenga-Hut, P.; Gross, A.; Clark, S.; Bassan, M.; Gilgun-Sherki, Y.; Mendzelevski, B.; Spiegelstein, O. Safety, Pharmacokinetics, and Pharmacodynamics of TV-1380, a Novel Mutated Butyrylcholinesterase Treatment for Cocaine Addiction, After Single and Multiple Intramuscular Injections in Healthy Subjects. *J. Clin. Pharmacol.* **2015**, *55*, 573−583.
(26) Nasser, A. F.; Fudala, P. J.; Zheng, B.; Liu, Y.; Heidbreder, C. A randomized, double-blind, placebo-controlled trial of RBP-8000 in cocaine abusers: pharmacokinetic profile of rbp-8000 and cocaine and effects of RBP-8000 on cocaine-induced physiological effects. *J. Addict. Dis.* **2014**, *33*, 289−302.
(27) Bencharit, S.; Morton, C. L.; Xue, Y.; Potter, P. M.; Redinbo, M. R. Structural basis of heroin and cocaine metabolism by a promiscuous human drug-processing enzyme. *Nat. Struct. Mol. Biol.* **2003**, *10* (5), 349−356.
(28) Brünger, A. T.; Karplus, M. Polar Hydrogen Positions in Proteins: Empirical Energy Placement and Neutron Diffraction Comparison. *Proteins: Struct., Funct., Genet.* **1988**, *4* (2), 148−156.
(29) Jorgensen, W. L. Quantum and Statistical Mechanical Studies of Liquids 0.10. Transferable Intermolecular Potential Functions for Water, Alcohols, and Ethers - Application to Liquid Water. *J. Am. Chem. Soc.* **1981**, *103* (2), 335−340.
(30) Neria, E.; Fischer, S.; Karplus, M. Simulation of Activation Free Energies in Molecular Systems. *J. Chem. Phys.* **1996**, *105* (5), 1902−1921.
(31) Brooks, B. R.; Brooks, C. L.; Mackerell, A. D.; Nilsson, L.; Petrella, R. J.; Roux, B.; Won, Y.; Archontis, G.; Bartels, C.; Boresch, S.; Caflisch, A.; Caves, L.; Cui, Q.; Dinner, A. R.; Feig, M.; Fischer, S.; Gao, J.; Hodoscek, M.; Im, W.; Kuczera, K.; Lazaridis, T.; Ma, J.; Ovchinnikov, V.; Paci, E.; Pastor, R. W.; Post, C. B.; Pu, J. Z.; Schaefer, M.; Tidor, B.; Venable, R. M.; Woodcock, H. L.; Wu, X.; Yang, W.; York, D. M.; Karplus, M. CHARMM: The Biomolecular Simulation Program. *J. Comput. Chem.* **2009**, *30* (10), 1545−1614.
(32) Field, M. J.; Bash, P. A.; Karplus, M. A Combined Quantum-Mechanical and Molecular Mechanical Potential for Molecular-Dynamics Simulations. *J. Comput. Chem.* **1990**, *11* (6), 700−733.
(33) Cui, Q.; Elstner, M.; Kaxiras, E.; Frauenheim, T.; Karplus, M. A QM/MM implementation of the self-consistent charge density functional tight binding (SCC-DFTB) method. *J. Phys. Chem. B* **2001**, *105* (2), 569−585.
(34) MacKerell, A. D.; Bashford, D.; Bellott, M.; Dunbrack, R. L.; Evanseck, J. D.; Field, M. J.; Fischer, S.; Gao, J.; Guo, H.; Ha, S.; Joseph-McCarthy, D.; Kuchnir, L.; Kuczera, K.; Lau, F. T. K.; Mattos, C.; Michnick, S.; Ngo, T.; Nguyen, D. T.; Prodhom, B.; Reiher, W. E.; Roux, B.; Schlenkrich, M.; Smith, J. C.; Stote, R.; Straub, J.; Watanabe, M.; Wiorkiewicz-Kuczera, J.; Yin, D.; Karplus, M. All-Atom Empirical Potential for Molecular Modeling and Dynamics Studies of Proteins. *J. Phys. Chem. B* **1998**, *102* (18), 3586−3616.
(35) Brooks, C. L.; Brunger, A.; Karplus, M. Active-Site Dynamics in Protein Molecules - A Stochastic Boundary Molecular-Dynamics Approach. *Biopolymers* **1985**, *24* (5), 843−865.
(36) Ryckaert, J. P.; Ciccotti, G.; Berendsen, H. J. C. Numerical-Integration of Cartesian Equations of Motion of a System with Constraints - Molecular-Dynamics of N-Alkanes. *J. Comput. Phys.* **1977**, *23* (3), 327−341.
(37) Schmidt, M. W.; Baldridge, K. K.; Boatz, J. A.; Elbert, S. T.; Gordon, M. S.; Jensen, J. H.; Koseki, S.; Matsunaga, N.; Nguyen, K. A.; Su, S. J.; Windus, T. L.; Dupuis, M.; Montgomery, J. A. General Atomic and Molecular Electronic-Structure System. *J. Comput. Chem.* **1993**, *14* (11), 1347−1363.
(38) Shao, Y.; Gan, Z.; Epifanovsky, E.; Gilbert, A. T. B.; Wormit, M.; Kussmann, J.; Lange, A. W.; Behn, A.; Deng, J.; Feng, X.; Ghosh, D.; Goldey, M.; Horn, P. R.; Jacobson, L. D.; Kaliman, I.; Khaliullin, R. Z.; Kuś, T.; Landau, A.; Liu, J.; Proynov, E. I.; Rhee, Y. M.; Richard, R. M.; Rohrdanz, M. A.; Steele, R. P.; Sundstrom, E. J.; Woodcock, H. L.; Zimmerman, P. M.; Zuev, D.; Albrecht, B.; Alguire, E.; Austin, B.; Beran, G. J. O.; Bernard, Y. A.; Berquist, E.; Brandhorst, K.; Bravaya, K. B.; Brown, S. T.; Casanova, D.; Chang, C.-M.; Chen, Y.; Chien, S. H.; Closser, K. D.; Crittenden, D. L.; Diedenhofen, M.; DiStasio, R. A.; Do, H.; Dutoi, A. D.; Edgar, R. G.; Fatehi, S.; Fusti-Molnar, L.; Ghysels, A.; Golubeva-Zadorozhnaya, A.; Gomes, J.; Hanson-Heine, M. W. D.; Harbach, P. H. P.; Hauser, A. W.; Hohenstein, E. G.; Holden, Z. C.; Jagau, T.-C.; Ji, H.; Kaduk, B.; Khistyaev, K.; Kim, J.; Kim, J.; King, R. A.; Klunzinger, P.; Kosenkov, D.; Kowalczyk, T.; Krauter, C. M.; Lao, K. U.; Laurent, A. D.; Lawler, K. V.; Levchenko, S. V.; Lin, C. Y.; Liu, F.; Livshits, E.; Lochan, R. C.; Luenser, A.; Manohar, P.; Manzer, S. F.; Mao, S.-P.; Mardirossian, N.; Marenich, A. V.; Maurer, S. A.; Mayhall, N. J.; Neuscamman, E.; Oana, C. M.; Olivares-Amaya, R.; O'Neill, D. P.; Parkhill, J. A.; Perrine, T. M.; Peverati, R.; Prociuk, A.; Rehn, D. R.; Rosta, E.; Russ, N. J.; Sharada, S. M.; Sharma, S.; Small, D. W.; Sodt, A.; Stein, T.; Stück, D.; Su, Y.-C.; Thom, A. J. W.; Tsuchimochi, T.; Vanovschi, V.; Vogt, L.; Vydrov, O.; Wang, T.; Watson, M. A.; Wenzel, J.; White, A.; Williams, C. F.; Yang, J.; Yeganeh, S.; Yost, S. R.; You, Z.-Q.; Zhang, I. Y.; Zhang, X.; Zhao, Y.; Brooks, B. R.; Chan, G. K. L.; Chipman, D. M.; Cramer, C. J.; Goddard, W. A.; Gordon, M. S.; Hehre, W. J.; Klamt, A.; Schaefer, H. F.; Schmidt, M. W.; Sherrill, C. D.; Truhlar, D. G.; Warshel, A.; Xu, X.; Aspuru-Guzik, A.; Baer, R.; Bell, A. T.; Besley, N. A.; Chai, J.-D.; Dreuw, A.; Dunietz, B. D.; Furlani, T. R.; Gwaltney, S. R.; Hsu, C.-P.; Jung, Y.; Kong, J.; Lambrecht, D. S.; Liang, W.; Ochsenfeld, C.; Rassolov, V. A.; Slipchenko, L. V.; Subotnik, J. E.; Van Voorhis, T.; Herbert, J. M.; Krylov, A. I.; Gill, P. M. W.; Head-Gordon, M. Advances in molecular quantum chemistry contained in the Q-Chem 4 program package. *Mol. Phys.* **2015**, *113* (2), 184−215.
(39) Liu, J. J.; Hamza, A.; Zhan, C.-G. Fundamental Reaction Mechanism and Free Energy Profile for (−)-Cocaine Hydrolysis Catalyzed by Cocaine Esterase. *J. Am. Chem. Soc.* **2009**, *131* (33), 11964−11975.
(40) Liu, J. J.; Zhan, C.-G. Reaction Pathway and Free Energy Profile for Cocaine Hydrolase-Catalyzed Hydrolysis of (−)-Cocaine. *J. Chem. Theory Comput.* **2012**, *8*, 1426−1435.
(41) Yao, Y.; Liu, J.; Zheng, F.; Zhan, C.-G. Reaction pathway for cocaine hydrolase-catalyzed hydrolysis of (+)-cocaine. *Theor. Chem. Acc.* **2016**, *135*, 15.
(42) Yao, Y.; Liu, J. J.; Zhan, C.-G. Why does the G117H mutation considerably improve the activity of human butyrylcholinesterase against sarin? Insights from quantum mechanical/molecular mechanical free energy calculations. *Biochemistry* **2012**, *51*, 8980−8992.
(43) Chen, X.; Fang, L.; Liu, J. J.; Zhan, C.-G. Reaction pathway and free energy profile for butyrylcholinesterase-catalyzed hydrolysis of acetylcholine. *J. Phys. Chem. B* **2011**, *115*, 1315−1322.
(44) Chen, X.; Fang, L.; Liu, J. J.; Zhan, C.-G. Reaction pathway and free energy profiles for butyrylcholinesterase-catalyzed hydrolysis of acetylthiocholine. *Biochemistry* **2012**, *51*, 1297−1305.
(45) Qiao, Y.; Han, K.; Zhan, C.-G. Reaction pathways and free energy profiles for cholinesterase-catalyzed hydrolysis of 6-monoacetylmorphine. *Org. Biomol. Chem.* **2014**, *12*, 2214−2227 (Cover Article).
(46) Qiao, Y.; Han, K. L.; Zhan, C.-G. Fundamental reaction pathway and free energy profile for butyrylcholinesterase-catalyzed hydrolysis of heroin. *Biochemistry* **2013**, *52*, 6467−6479.

DOI: 10.1021/acs.molpharmaceut.8b00354
Mol. Pharmaceutics 2018, 15, 3871−3880

(47) Wei, D.; Huang, X.; Qiao, Y.; Rao, J.; Wang, L.; Liao, F.; Zhan, C.-G. Catalytic Mechanisms for Cofactor-Free Oxidase-Catalyzed Reactions: Reaction Pathways of Uricase-Catalyzed Oxidation and Hydration of Uric Acid. *ACS Catal.* **2017**, *7*, 4623−4636.
(48) Yao, J.; Yuan, Y.; Zheng, F.; Zhan, C.-G. Unexpected reaction pathway for butyrylcholinesterase-catalyzed inactivation of 'hunger hormone' ghrelin. *Sci. Rep.* **2016**, *6*, 22322.
(49) Elstner, M. The SCC-DFTB method and its application to biological systems. *Theor. Chem. Acc.* **2006**, *116* (1−3), 316−325.
(50) Brooks, B. R.; Bruccoleri, R. E.; Olafson, B. D.; States, D. J.; Swaminathan, S.; Karplus, M. CHARMM - A Program for Macromolecular Energy, Minimization, and Dynamics Calculations. *J. Comput. Chem.* **1983**, *4* (2), 187−217.
(51) Woodcock, H. L.; Hodošček, M.; Gilbert, A. T.; Gill, P. M.; Schaefer, H. F.; Brooks, B. R. Interfacing Q-Chem and CHARMM to perform QM/MM reaction path calculations. *J. Comput. Chem.* **2007**, *28* (9), 1485−1502.
(52) Torrie, G. M.; Valleau, J. P. Monte-Carlo Free-Energy Estimates Using Non-Boltzmann Sampling - Application to Subcritical Lennard-Jones Fluid. *Chem. Phys. Lett.* **1974**, *28* (4), 578−581.
(53) Kumar, S.; Bouzida, D.; Swendsen, R. H.; Kollman, P. A.; Rosenberg, J. M. The Weighted Histogram Analysis Method for Free-Energy Calculations on Biomolecules 0.1. The Method. *J. Comput. Chem.* **1992**, *13* (8), 1011−1021.
(54) Chen, X.; Zheng, X.; Ding, K.; Zhou, Z.; Zhan, C.-G.; Zheng, F. A quantitative LC−MS/MS method for simultaneous determination of cocaine and its metabolites in whole blood. *J. Pharm. Biomed. Anal.* **2017**, *134*, 243−251.
(55) Imai, T. Human Carboxylesterase Isozymes: Catalytic Properties and Rational Drug Design. *Drug Metab. Pharmacokinet.* **2006**, *21* (3), 173−185.
(56) Yao, J.; Guo, H.; Chaiprasongsuk, M.; Zhao, N.; Chen, F.; Yang, X.; Guo, H. Substrate-Assisted Catalysis in the Reaction Catalyzed by Salicylic Acid Binding Protein 2 (SABP2), a Potential Mechanism of Substrate Discrimination for Some Promiscuous Enzymes. *Biochemistry* **2015**, *54* (34), 5366−5375.
(57) Brzezinski, M. R.; Abraham, T. L.; Stone, C. L.; Dean, R. A.; Bosron, W. F. Purification and characterization of a human liver cocaine carboxylesterase that catalyzes the production of benzoylecgonine and the formation of cocaethylene from alcohol and cocaine. *Biochem. Pharmacol.* **1994**, *48*, 1747−1755.
(58) Pindel, E. V.; Kedishvili, N. Y.; Abraham, T. L.; Brzezinski, M. R.; Zhang, J.; Dean, R. A.; Bosron, W. F. Purification and Cloning of a Broad Substrate Specificity Human Liver Carboxylesterase That Catalyzes the Hydrolysis of Cocaine and Heroin. *J. Biol. Chem.* **1997**, *272*, 14769−14775.
(59) Chen, X.; Huang, X.; Geng, L.; Xue, L.; Hou, S.; Zheng, X.; Brimijoin, S.; Zheng, F.; Zhan, C.-G. Kinetic characterization of a cocaine hydrolase engineered from mouse butyrylcholinesterase. *Biochem. J.* **2015**, *466*, 243−251.
(60) Ross, M. K.; Borazjani, A.; Wang, R.; Crow, J. A.; Xie, S. Examination of the carboxylesterase phenotype in human liver. *Arch. Biochem. Biophys.* **2012**, *522*, 44−56.
(61) Garrett, B. C.; Truhlar, D. G. *Transition State Theory in Encyclopedia of Computational Chemistry*; John Wiley & Sons: Chichester, UK, 1998.

DOI: 10.1021/acs.molpharmaceut.8b00354
Mol. Pharmaceutics 2018, 15, 3871−3880